SF2A 2022
J. Richard, A. Siebert, E. Lagadec, N. Lagarde, O. Venot, J. Malzac, J.-B. Marquette, M. N'Diaye, D. Briot (eds)

CHALLENGING THE DENSE CORE IDENTIFICATION IN A STRONGLY DYNAMICAL, MAGNETIZED AND TURBULENT REGION OF THE PIPE NEBULA.

S. Delcamp[1] and P. Hily-Blant[1]

Abstract. The Pipe Nebula is a nearby filamentary shaped molecular cloud in which star formation is concentrated in the western end of the cloud known as B59, while the eastern part has no star formation. The morphology of the projected magnetic fields is well constrained through both extinction and emission dust polarization measurements, showing field lines perpendicular to the main axis of the molecular cloud. Yet, field lines are much less dispersed in the non–star-forming part of the cloud compared to a less ordered B59. Furthermore, kinematic studies of the eastern part show two velocity components, 3.5 km/s apart in projected velocity, which may be indicative of colliding flows. The eastern end of the Pipe Nebula thus constitutes a highly turbulent, strongly magnetized test case to be compared with numerical simulations.

We present the first ^{12}CO(1-0), sub-arcmin resolution (32" HPBW) large-scale (0.5x0.7 deg) map of the converging flow region, obtained with the IRAM-30m antenna. The result confirms the extremely dynamic nature of the region. The ^{12}CO(1-0), emission line covers 4.5 km/s with up to five velocity components connected in physical and velocity spaces. We performed longer integration towards dense cores identified based on dust extinction and emission, in ^{12}CO(1-0), (2-1), and isotopologues, as well as HCO^+, N_2H^+, HCN, and CN. The non-detection rate of these species suggest that these targets are unlikely to be dense cores. This is also consistent with low visual extinctions based on CO column density estimates. This suggests some limitation of automatic core detection methods based on dust in highly turbulent clouds, with consequences on the core mass function in such environments. The large area mapped in ^{12}CO also offers the opportunity to explore the relative orientation of gaseous filaments with respect to the (projected) magnetic field lines.

Keywords: ISM: clouds, ISM: molecules, ISM: structure, ISM: evolution, ISM: individual (Pipe), ISM: magnetic fields, turbulence

1 Introduction

Explaining the star formation rate is critical to understand the star formation history of the universe. Detailed studies of galactic molecular clouds provide unique means to explore the interplay between gas dynamics, magnetic fields, gravity, chemistry, and radiation. It has become clear over the last decade that the so-called gas depletion time in molecular clouds is much longer that the dynamical timescale: whether the star formation process is intrinsically slow or rather fast but inefficient remains an open question, though being a crucial one (Chevance et al. 2020; Girichidis et al. 2020; Hennebelle & Falgarone 2012). Comparison of three-dimensional (3D) direct numerical simulations (DNS) of multi-phase turbulent gaseous clouds to spectral line maps of molecular clouds is expected to provide strong constraints. The present work focuses on a non-star-forming region of the Pipe Molecular cloud, in the strongly turbulent and strongly magnetized regime.

2 A strongly turbulent, magnetized, non-star forming region

Using the 30m-IRAM telescope, we have mapped in ^{12}CO(1-0) a $0.5^o \times 0.7^o$ area in the Pipe Molecular cloud; the region is located at the overlap of the two large-scale velocity components identified previously by Onishi et al. (1999) (see Fig. 1). The region was also chosen for the large dynamic in dust emission, in view of studying the formation of dense, bright filaments from tenuous, faint ones. The mapping was complemented by pointed,

[1] Univ. Grenoble Alpes, CNRS, IPAG, 38000 Grenoble, France

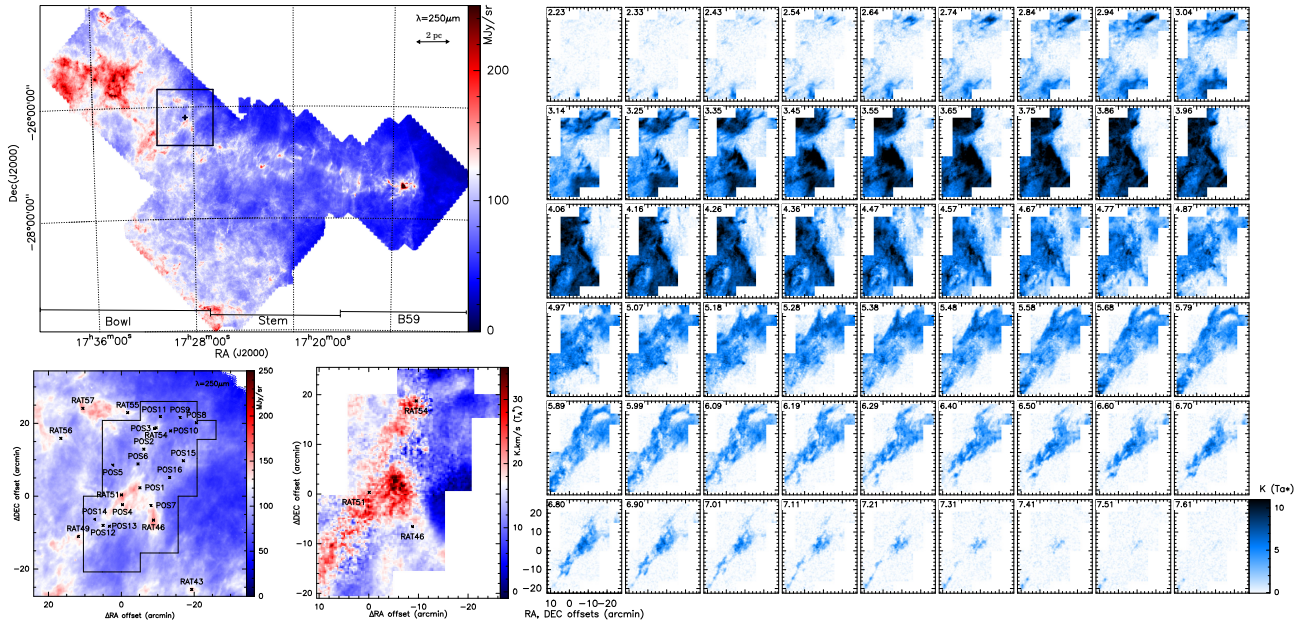

Fig. 1. Top-Left: Herschel-SPIRE dust map at 250μm. The region presented in this paper is outlined as a black rectangle. **Bottom left:** zoom over the region considered. The black contour delineates the region observed in ^{12}CO(1-0). Dense cores candidates are named after Rathborne et al. (2009) nomenclature. Pointed observations not in the Rathborne et al. catalog are named as POSi (1 to 16). **Bottom right:** Velocity integrated map of the ^{12}CO(1-0) between 2.2 and 7.5 km/s. The emission is in K.km/s ($T_A^\star$ scale). **Right:** Channel map of the ^{12}CO(1-0) emission.

multi-line observations towards dense cores identified in extinction maps (Alves et al. 2008; Rathborne et al. 2009). Other positions corresponding to bright peaks in the Herschel/SPIRE dust emission map have also been observed. This is motivated by earlier studies concluding to a gradient in the evolutionary stage of cores in this cloud (Frau et al. 2010).

The Pipe molecular cloud is nearby ($d = 163 \pm 5$pc, Dzib et al. 2018) and shows multiple dust filamentary structures across ~ 20 pc on the Herschel-SPIRE map at 250 μm (Griffin et al. 2010) presented in top of Fig. 1. It was divided into three regions (Alves et al. 2008): B59 with star formation, the Stem with tenuous filaments and few dense cores, and the Bowl with younger dense cores and tenuous or dense filaments. The Pipe Nebula also presents the particularity to have a magnetic field orientation projected into the plane-of-sky (B_{pos}) well perpendicular to its main axis at large scale ($\sim 143^o$, Planck Collaboration et al. 2015). At small scales, Franco et al. (2010) showed a highly disperse B_{pos} close to B59 (dispersion of $\sim 25^o$ across a 12'x12' region), but well oriented at the Bowl-to-Stem limit ($\sim 2^o$) and moreover coherent with the large-scale orientation found with Planck ($\sim 164^o$) . The Bowl-to-Stem limit also presents the superposition of two large-scale filamentary structures, centered at 3.5 and 5 km/s in ^{13}CO(1-0) (Onishi et al. 1999; Muench et al. 2007; Frau et al. 2015).

Reviewed by Skalidis et al. (2021) for compressible and magnetized turbulence regions, the modified Davis-Chandrasekhar-Fermi method gives access to the magnetic field intensity if having the H_2 density (n_{H_2}=1(3)cm^{-2}), B_{pos} dispersion ($\delta\phi$=2.54^o , Franco et al. 2010) and velocity dispersion ($\Delta V^{^{12}\mathrm{CO}} = 4$km/s): $\|B\| \approx 314.5\ \mu G$. Based on Crutcher et al. (2010), this is a high value for molecular clouds. Thus, the thermal to magnetic pressure ratio is $\beta = 1E(-3)$ assuming a temperature of 10K and the same density as before. The Mach number is besides equal to 14. This region of the Pipe nebula is then highly magnetized, with a domination of the magnetic pressure over thermal ones.

3 Low-brightness filamentary structures

The channel map of Fig. 1 shows that the ^{12}CO emission covers a broad velocity range, from 2 to 7.8 km/s. Two overlapping large-scale structures, almost perpendicular to each other, are easily seen: one, at velocities below $\approx 4.5\,\mathrm{kms}^{-1}$ is oriented North-East to South-West, and is the brightest in ^{12}CO, with a peak intensity up to $T_A^\star = 13$K. This will be referred to as the low-velocity structure (LVS). The other is easily visible at velocities

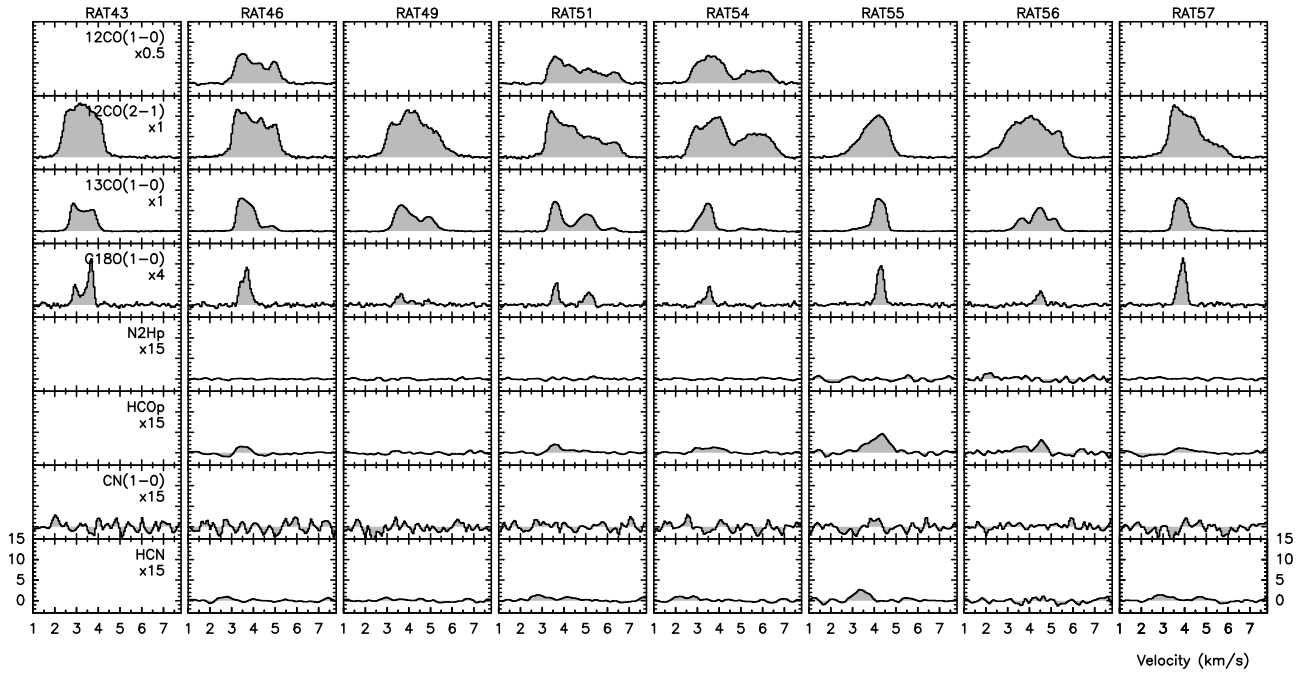

Fig. 2. Spectra towards the core candidates of Rathborne et al. (2009). The intensity is given in K (Tmb scale). For a better visualization, intensities are multiplied by a factor specified on the name of the transition.

above $5\,\mathrm{kms}^{-1}$: its peak intensity is ≈ 5 K, half that at lower velocities. We will refer to it as the high-velocity structure (HVS). The channel map clearly shows that these two structures overlap at velocities $\approx 4.5\,\mathrm{kms}^{-1}$, ruling out the possibility that they correspond to non-related physical structures.

The LVS and HVS can be associated to the large scale ones formerly identified by Onishi et al. (1999). Nevertheless, the present high-spatial resolution map shows multiple faint filamentary structures. Eye inspection of the channel map, we have identified ≈ 300 structures based on the following criteria: a structure remains spatially coherent over more than 0.2 km/s. The transverse size of these structures is obtained by Gaussian fitting the emission averaged over their velocity coverage. For each structure, we thus obtain the length, transverse size (FWHM), velocity coverage, and position angle (counted positive from North to East, IAU convention). In addition, using the H_2 column density map produced by Peretto et al. (2012) based on Herschel/SPIRE maps, we have estimated the column density of each filament. This result is to be taken with caution because of potential projection effects of the dust emission; to this regard, the identification based on ^{12}CO emission is more robust because the velocity information mitigates (part of) the line-of-sight confusion. The range of column densities span from 1.4E21 to 3.6E21 cm^{-2}, with 52% lower than 2E21 cm^{-2}.

Among the ~ 300 structures, 159 have an aspect ratio larger than two and may thus be filamentary structures. Except for ≈ 10 structures, they all have a longitudinal size lower than 0.4 pc, and 72 % of the structures have a transverse size lower than 0.1 pc, while the angular resolution is equal to 25 mpc (assuming a distance of 163pc). Furthermore, 46% of the structures are parallel with the average position angle of the projected magnetic fields. In contrast, 12% of the structures are perpendicular to the magnetic field.

4 Challenging dense core identification based on extinction maps

Figure 2 shows the result of the multi-line observations towards the positions identified as dense cores based on extinction maps by Lombardi et al. (2006); Muench et al. (2007); Rathborne et al. (2008, 2009). Among the 8 cores, 3 (RAT46, 51 and 54) are also covered in the ^{12}CO(1-0) map. The ^{12}CO(2-1), ^{13}CO(1-0) and C^{18}O(1-0) lines are detected in emission towards all cores. With an averaged 3σ RMS of 0.04 K (Tmb), no N_2H^+ has been detected. HCO^+ was detected in 5 of the cores, while HCN was found in 3 dense core positions but close to the 3σ RMS.

The ^{13}CO(1-0) shows multiple velocity components which are not always well separated (compare RAT43 and RAT51). In such instances, the C^{18}O(1-0) usually displays well separated components. However, not all

^{13}CO lines have a C^{18}O counterpart: thus, towards RAT51, the weak ^{13}CO line at $\approx$ 6kms^{-1} is not seen in C^{18}O. This is a standard behavior which is usually understood in terms of column density that is, opacity. Therefore, the combination of the ^{12}CO, ^{13}CO, and C^{18}O lines allows the CO column density to be estimated, under simplifying assumptions on the rotational levels excitation and radiative transfer.

We estimated column density of these objects following the usual steps leading from line intensities ratio to column density ratios using radiative transfer equations. Based on the C^{18}O optically thin lines, we derive the central line opacity and, adopting isotopic ratios between CO isotopologs (X(C^{18}O):X(^{13}CO):X(^{12}CO) = 1:7:500 Henkel & Mauersberger 1993; Milam et al. 2005), we have estimated the CO column density. These were converted into a H_2 column density by assuming a CO:H_2 abundance of 8.3E-5. This is probably a lower limit at low Av, where a value of 1.4E-4 is more likely. Thus, the H_2 column density are indeed upper limits. Visual extinctions are derived using $N_H/A_V = 1.8(21)\,\mathrm{cm}^{-2}/\mathrm{mag}$. Among the cores in our survey, RAT57 has the highest extinction, $A_V = 2.2$ mag, three of them have values around 1.85 mag (RAT43, RAT51 and RAT55), while the remaining four cores have $A_V < 1$ mag. Compared to Rathborne et al. (2009), only RAT57 is in concordance with their results. RAT55 is 1.5 times lower, RAT43, RAT49, RAT51, and RAT56 are 2 times lower, RAT54 4 times, and 10 times for RAT46.

Together with the non-detection of N_2H^+ towards any of the cores in the sample, the low column density (or extinction) towards these locations suggest that they are not actual dense cores ($A_V \geq$ 4 mag, Bergin & Tafalla 2007).

5 Conclusions

We have presented the first high-resolution map of the ^{12}CO(1-0) emission of the Pipe molecular cloud. The chosen region corresponds to a highly dynamic, magnetized and turbulent site, a perfect study case for numerical simulations. Bright and faint filaments are seen in dust emission, providing an ideal case to study the formation of dense filaments.

Our 1260 arcmin^2 ^{12}CO survey coincides with two overlapping large scale structures (LVS and HVS) separated by 3.5 kms^{-1}, which could be colliding clouds. The LVS and HVS are almost perpendicular to each other, with the HVS being aligned with the projected magnetic fields, B_{pos}. Our survey contains $\approx$ 160 filamentary structures which were identified in velocity space to mitigate projection effects to which continuum emission maps are exposed. In total, 46% of these are found parallel to B_{pos}, and 12% perpendicular to it, indicating that $\approx$ 40% are neither parallel nor perpendicular. These could correspond to the transition between low- to high-density structures (Soler & Hennebelle 2017). The estimated higher-limit H_2 column density of these filaments are found to be between 1.4 and 3.6 (21) cm^{-2}. While these values could be indications of a region transiting from tenuous to dense gas structures, the dissection of the spectra across the region suggests an overlap of structure along the line of sight, as suggested also by the velocity channel map.

Furthermore, a multi-line analysis of dense cores formerly identified from extinction maps provide low gas column densities that are not compatible with these sources being dense cores. This is also supported by the non-detection of N_2H^+. This preliminary study calls for additional spectral line observations but already casts doubts on automatic detection of cores based on extinction maps in regions similar to the one studied here.

This region thus presents particularities of a highly dynamical, magnetized and turbulent field, while not forming stars. At the contrary, the Polaris flare is a cloud that forms stars, with signs of turbulent dissipation linked to the superposition of velocity structures (Hily-Blant et al. 2008; Hily-Blant & Falgarone 2009), at $\sim$ 355 pc from us (Panopoulou et al. 2022), but with a disperse B_{pos}. A direct comparison between chemical and physical properties of the Polaris flare and the Pipe Nebula could highlight important effects of filament and dense core formation, and allow a better understanding of the transition from diffuse to dense molecular clouds.

This research has received funding from the European Research Council through the Advanced Grant MIST (FP7/2017-2020, No 742719). This work is based on observations carried out under project number 030-21 and 126-21 with the IRAM-30m telescope. IRAM is supported by INSU/CNRS (France), MPG (Germany) and IGN (Spain). We want to specifically thank the help received by all the IRAM-30m staff during these two sessions of observations, in remote as in site.

References

Alves, F. O., Franco, G. A. P., & Girart, J. M. 2008, A&A, 486, L13

Bergin, E. & Tafalla, M. 2007

Chevance, M., Kruijssen, J. M. D., Vazquez-Semadeni, E., et al. 2020, Space Sci Rev, 216, 50

Crutcher, R. M., Wandelt, B., Heiles, C., Falgarone, E., & Troland, T. H. 2010, ApJ, 725, 466
Dzib, S. A., Loinard, L., Ortiz-León, G. N., Rodríguez, L. F., & Galli, P. A. B. 2018, ApJ, 867, 151
Franco, G. A. P., Alves, F. O., & Girart, J. M. 2010, ApJ, 723, 146
Frau, P., Girart, J. M., Alves, F. O., et al. 2015, A&A, 574, L6
Frau, P., Girart, J. M., Beltrán, M. T., et al. 2010, ApJ, 723, 1665
Girichidis, P., Offner, S. S. R., Kritsuk, A. G., et al. 2020, arXiv:2005.06472 [astro-ph]
Griffin, M. J., Abergel, A., Abreu, A., et al. 2010, A&A, 518, L3
Henkel, C. & Mauersberger, R. 1993, Astronomy & Astrophysics
Hennebelle, P. & Falgarone, E. 2012, Astron Astrophys Rev, 20, 55
Hily-Blant, P. & Falgarone, E. 2009, A&A, 500, L29
Hily-Blant, P., Falgarone, E., & Pety, J. 2008, A&A, 481, 367
Lombardi, M., Alves, J., & Lada, C. J. 2006, A&A, 454, 781
Milam, S. N., Savage, C., Brewster, M. A., Ziurys, L. M., & Wyckoff, S. 2005, ApJ, 634, 1126
Muench, A. A., Lada, C. J., Rathborne, J. M., Alves, J. F., & Lombardi, M. 2007, ApJ, 671, 1820
Onishi, T., Kawamura, A., Abe, R., et al. 1999
Panopoulou, G. V., Clark, S. E., Hacar, A., et al. 2022, A&A, 657, L13
Peretto, N., André, P., Könyves, V., et al. 2012, A&A, 541, A63
Planck Collaboration, Ade, P. A. R., Aghanim, N., et al. 2015, A&A, 576, A104
Rathborne, J. M., Lada, C. J., Muench, A. A., et al. 2009, ApJ, 699, 742
Rathborne, J. M., Lada, C. J., Muench, A. A., Alves, J. F., & Lombardi, M. 2008, ASTROPHYS J SUPPL S, 174, 396
Skalidis, R., Sternberg, J., Beattie, J. R., Pavlidou, V., & Tassis, K. 2021, A&A, 656, A118
Soler, J. D. & Hennebelle, P. 2017, A&A, 607, A2